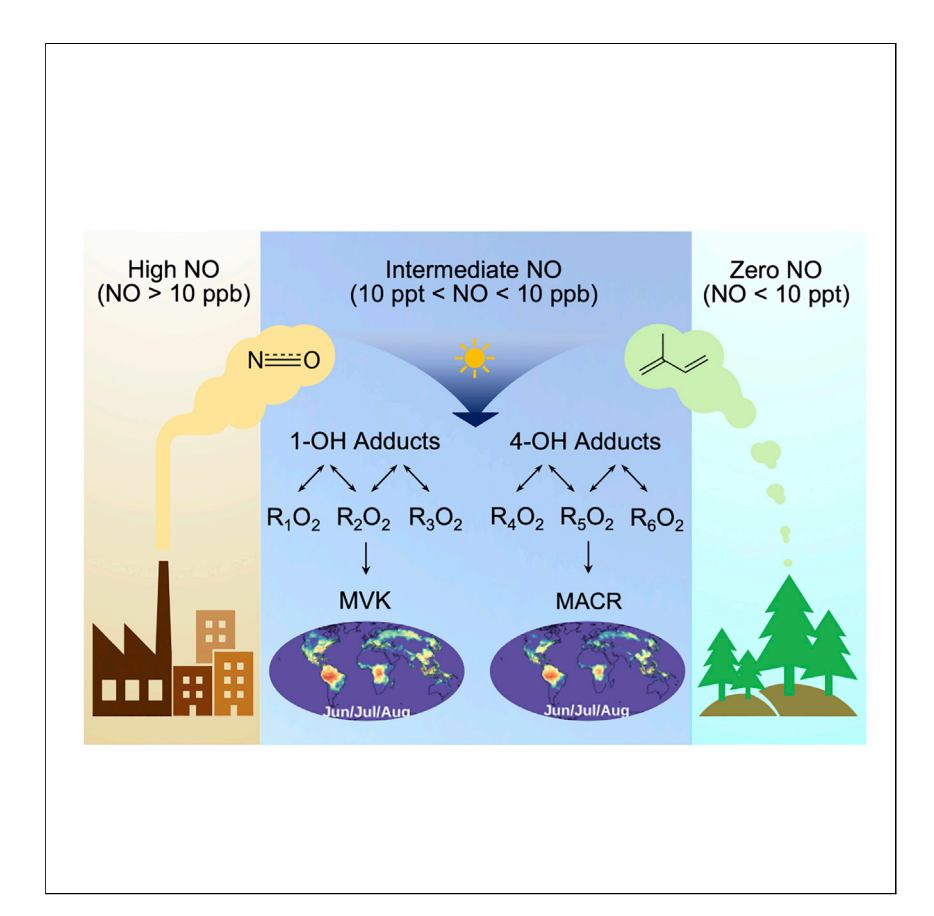




Article

Probing isoprene photochemistry at atmospherically relevant nitric oxide levels



We probe the photochemistry of isoprene, which is the dominant nonmethane hydrocarbon emitted to the atmosphere, in a chemical regime characterized by parts-per-trillion nitrogen oxides (NO $_{\rm x}$), a regime that becomes increasingly prevalent owing to efforts taken to reduce anthropogenic NO $_{\rm x}$ emissions worldwide. We show the isoprene photooxidation pathway is remarkably sensitive to NO $_{\rm x}$ concentrations, which results in an appreciable perturbation in the global distributions of isoprene oxidation products with associated impacts on the production of ozone and particulate matter in the atmosphere.

Xuan Zhang, Siyuan Wang, Eric C. Apel, ..., Paul O. Wennberg, Geoffrey S. Tyndall, John J. Orlando

xzhang87@ucmerced.edu (X.Z.) orlando@ucar.edu (J.J.O.)

Highlights

Formation of MACR and MVK from isoprene photooxidation is enhanced with sub-ppb NO

Accelerated production of MACR and MVK results from the isoprene peroxy interconversion

Isoprene peroxy interconversion is prevalent in many vegetated continents over the globe



Zhang et al., Chem *8*, 1–16 December 8, 2022 © 2022 Elsevier Inc. https://doi.org/10.1016/j.chempr.2022.08.003

Chem



Article

Probing isoprene photochemistry at atmospherically relevant nitric oxide levels

Xuan Zhang,^{1,11,12,*} Siyuan Wang,^{2,10,11} Eric C. Apel,³ Rebecca H. Schwantes,^{2,10} Rebecca S. Hornbrook,³ Alan J. Hills,³ Kate E. DeMarsh,¹ Zeyi Moo,¹ John Ortega,³ William H. Brune,⁴ Roy L. Mauldin III,⁵ Christopher A. Cantrell,⁶ Alexander P. Teng,⁷ Donald R. Blake,⁸ Teresa Campos,³ Bruce Daube,⁹ Louisa K. Emmons,³ Samuel R. Hall,³ Kirk Ullmann,³ Steven C. Wofsy,⁹ Paul O. Wennberg,⁷ Geoffrey S. Tyndall,³ and John J. Orlando^{3,*}

SUMMARY

The reactive chemistry of isoprene, which is the dominant hydrocarbon in biogenic emissions, has a controlling influence on the composition and cleansing capacity of the global atmosphere. Despite decades of research, isoprene continues to offer surprises in its atmospheric chemistry, particularly in environments with low-to-moderate levels of nitrogen oxides (NO_x). Here, we probe the isoprene photochemical oxidation in this "intermediate-NO_x" regime by examining the yield distributions of two major oxidation products, i.e., methacrolein and methyl vinyl ketone, using chamber experiments and aircraft measurements. Such a dataset provides strong constraints on the kinetics of the isoprene peroxy radical interconversion—a newly discovered mechanism that essentially governs the isoprene oxidation carbon flow. Insights from measurement-model comparisons further reveal an efficient operation of this mechanism across all the vegetated continents over the globe, constantly modulating the radical cycling and contributing to the formation of ozone and organic aerosols in the atmosphere.

INTRODUCTION

Biogenic emissions from terrestrial vegetation account for approximately 90% of the volatile organic compounds (VOCs) in Earth's atmosphere. Isoprene (2-methyl-1,3-butadiene), a five-carbon conjugated diene, is the dominant VOC of biogenic origin, with global emission estimates of $\sim\!500-750\, Tg\, C$ year $^{-1}$. Isoprene is highly reactive toward atmospheric oxidants, in particular the hydroxyl radical (OH), with an average lifetime of only 1 h against OH-initiated oxidation ($\tau_{OH}=1.4\, h$ for [OH] = 2 \times 106 molecules cm $^{-3}$ at T = 298 K). Owing to its large flux and high reactivity, the oxidative chemistry of isoprene exerts profound influences on the composition of the global atmosphere—modulating the balance of hydrogen oxide radicals (HO_x), $^{4-6}$ perturbing the cycling of reactive nitrogen, 7,8 and contributing to the formation of ozone and secondary organic aerosols. $^{9-15}$

The atmospheric photooxidation of isoprene is initiated by the addition of an OH radical to the unsaturated carbon backbone, yielding four distinct OH-adducts (Figure 1). 16 The OH addition to the terminal carbons (i.e., 1-OH-adduct and 4-OH-adduct) has been shown to dominate the overall carbon flow from isoprene. 17 Following collisional thermalization, each OH-adduct adds O_2 to produce a

THE BIGGER PICTURE

Isoprene is the most abundantly produced biogenic volatile organic compound on Earth. Over decades of research, the atmospheric chemistry of isoprene has been well studied under polluted urban conditions characterized by hundreds of parts-per-billion nitrogen oxides. With effective measures taken to reduce the anthropogenic emissions of nitrogen oxides worldwide, chemical regimes at play in the atmosphere are gradually transitioning from the polluted settings to environments with diminishing human influence. Here, by integrating chamber experiments, aircraft measurements, and model simulations, we demonstrate that in this transitional chemical regime, isoprene is photochemically oxidized through a mechanism that is remarkably different from our traditional understanding. We show that this mechanism operates competitively in the present atmosphere and constantly impacts the chemical composition and cleansing capacity of the atmosphere.





Figure 1. Reaction scheme for the formation of MACR and MVK from the OH-initiated oxidation of isoprene

The OH addition to the unsaturated carbon backbone of isoprene yields four structurally distinct OH-adducts, which further add O_2 at either the β or δ position to form two β -ISOPOO and four δ -ISOPOO peroxy radical isomers. The OH-adducts to the inner carbon represent a negligible fraction of the isoprene reactivity, and their following chemistry is not considered herein.

population of isoprene peroxy radicals (ISOPOO), the fate of which depends on the level of nitric oxide (NO). 18 In the absence of NO, ISOPOO radicals react primarily with HO $_2$ giving rise to isoprene hydroxy hydroperoxides. In the presence of elevated NO, the primary fate of ISOPOO radicals is to react with NO generating a number of first-generation products, including methacrolein (MACR) and methyl vinyl ketone (MVK) that dominate the reaction fluxes of the 4-OH and 1-OH systems, respectively. The formation of MACR and MVK from isoprene photooxidation under high-NO conditions (>300 parts per billion [ppb]) has been the subject of extensive chamber studies over the past few decades, with reported yields of 23.5% \pm 4.5% and 34.3% \pm 9.7%, respectively. $^{19-24}$ This branching provides crucial information on the atmospheric degradation mechanism of isoprene and has been translated into robust parameterizations in chemical transport models for the assessment of the impact of isoprene photochemistry on the oxidizing capacity and ozone formation in polluted environments.

The traditionally rationalized fate of ISOPOO radicals, however, has been challenged by recent studies. Theoretical calculations by Peeters et al.^{25,26} have revealed that the ISOPOO radicals readily eliminate O2 to regenerate the initial OH-adducts on timescales faster than the bimolecular processes under atmospherically relevant NO and HO2 levels (tens to hundreds of parts per trillion [ppt]). As such, the repetitive O₂ addition and dissociation process constantly interconvert different ISOPOO isomers, which eventually establish a thermal equilibrium distribution in the atmosphere. The proposed interconversion of ISOPOO isomers was later demonstrated by Teng et al. 17 with a novel analysis of isomer-specific yields of a selection of first-generation oxidation products under a range of peroxy bimolecular lifetimes. The consequence of such a highly dynamic system is the varying population fractions of ISOPOO isomers—and their corresponding reaction products—that ultimately depend on the dominant peroxy radical removal channel. It is therefore expected that NO plays a crucial role in modulating the distribution of isoprene oxidation products, including MACR and MVK: under "high-NO" conditions (NO > 10 ppb), the yields of MACR and MVK are determined by the initial kinetic distribution of ISOPOO radicals, whereas at "low-to-moderate NO" levels (10 ppt < NO < 10 ppb), the production of MACR and MVK is a synergistic result of competing reaction pathways that govern the fate of their precursor β -ISOPOO radicals (see the molecular structure in Figure 1). With effective measures taken to reduce the anthropogenic emissions of nitrogen oxides (NO_x) worldwide, the chemical regimes at play in the atmosphere are gradually transitioning from highly polluted urban settings to environments with diminishing anthropogenic influence, where the photochemistry of isoprene is no longer adequately described by the

¹Department of Life and Environmental Sciences, University of California, Merced, CA, USA

²Cooperative Institute for Research in Environmental Sciences, University of Colorado, Boulder, CO, USA

³Atmospheric Chemistry Observations & Modeling Laboratory, National Center for Atmospheric Research, Boulder, CO, USA

⁴Department of Meteorology and Atmospheric Science, Pennsylvania State University, University Park, PA, USA

⁵Department of Atmospheric and Oceanic Sciences, University of Colorado, Boulder, CO,

⁶Laboratoire Interuniversitaire des Systèmes Atmosphériques (LISA), Creteil, France

⁷Division of Geological and Planetary Sciences, Division of Engineering and Applied Science, California Institute of Technology, Pasadena, CA, IISA

⁸Department of Chemistry, University of California, Irvine, CA, USA

⁹John A. Paulson School of Engineering and Applied Sciences, Harvard University, Cambridge, MA, USA

¹⁰Chemical Sciences Laboratory, National Oceanic and Atmospheric Administration, Boulder, CO, USA

¹¹These authors contributed equally

12Lead contact

*Correspondence: xzhang87@ucmerced.edu (X.Z.), orlando@ucar.edu (J.J.O.)

https://doi.org/10.1016/j.chempr.2022.08.003





classic mechanism developed under "high-NO" chamber conditions. A mechanistic understanding of isoprene degradation pathways under this emerging chemical regime is thereby of crucial importance in accurate simulations of the budget of ozone and aerosols—and their health and climate consequences—from local to global scales.

In this study, we investigate the production of MACR and MVK from isoprene photooxidation through an integration of chamber experiments, aircraft measurements, and model simulations. Measurements of these two major first-generation products over a wide range of atmospherically relevant NO and HO2 levels allow for an indepth diagnosis of the operating degradation mechanism of isoprene in the atmosphere. Our chamber results reveal that the production of MVK is enhanced by up to a factor of two as NO approaches to \sim 100 ppt level, at which the interconversion of ISOPOO isomers outcompetes their bimolecular reactions. MACR formation at sub-ppb NO level, on the other hand, is rather limited as the result of an isomerization pathway that dominates the fate of the MACR-forming ISOPOO isomer. Aircraft observations conducted over North America further provide validation that the isoprene peroxy dynamics effectively regulate the spatial distributions of MACR and MVK in regions with intertwined biogenic and anthropogenic activities. By incorporating this observationally constrained ISOPOO kinetics in a global transport model, we show a remarkable increase in the surface concentrations of MACR and MVK across all vegetated continents of the world. Such a widespread shift suggests that the ISOPOO interconversion chemistry is prevailing in the present atmosphere and constantly impacts the radical cycling efficiency and the production of ozone and organic aerosols.

RESULTS AND DISCUSSION

Yields of MACR and MVK as a dependence of NO levels

A series of chamber experiments was conducted in the continuous-flow steady-state mode, with each experiment simulated by a box model operating with chemistry taken from the Master Chemical Mechanism (MCMv3.3.1, http://mcm. york.ac.uk). The observed and simulated temporal profiles of NO_x, O₃, and isoprene are shown in Figure S1. At steady state, their predicted concentrations agree within 8.4%, 5.7%, and 18.2%, respectively, with corresponding measurements, thereby providing robust constraints on the quantitative estimation of free radicals in the reaction system, as discussed shortly. To calculate the molar yield of MACR ($Y_{MACR \leftarrow OH}$) from the OH-oxidation pathway, six reactions as its sources (OH+ISOP, O₃+ISOP, and NO₃+ISOP) and sinks (OH+MACR, O₃+MACR, and NO₃+MACR) are considered. At steady state, two mass conservation equations are satisfied:

$$\frac{d[ISOP]_{ss}}{dt} = [ISOP]_{0}/\tau - [ISOP]_{ss}/\tau - k_{ISOP+OH}[OH]_{ss}[ISOP]_{ss}$$

$$- k_{ISOP+O_{3}}[O_{3}]_{ss}[ISOP]_{ss} - k_{ISOP+NO_{3}}[NO_{3}]_{ss}[ISOP]_{ss} = 0$$
 (Equation 1)
$$\frac{d[MACR]_{ss}}{dt} = Y_{MACR\leftarrow OH}k_{ISOP+OH}[OH]_{ss}[ISOP]_{ss} + Y_{MACR\leftarrow O_{3}}k_{ISOP+O_{3}}[O_{3}]_{ss}[ISOP]_{ss}$$

$$+ Y_{MACR\leftarrow NO_{3}}k_{ISOP+NO_{3}}[NO_{3}]_{ss}[ISOP]_{ss} - k_{MACR+OH}[OH]_{ss}[MACR]_{ss}$$

$$- k_{MACR+O_{3}}[O_{3}]_{ss}[MACR]_{ss} - k_{MACR+NO_{3}}[NO_{3}]_{ss}[MACR]_{ss}$$

$$- [MACR]_{ss}/\tau = 0,$$
 (Equation 2)





where [ISOP]_{ss} and [MACR]_{ss} are the measured steady-state concentrations of isoprene and MACR, respectively; [ISOP]₀ is the measured initial concentration of isoprene; [O₃]_{ss} is the measured steady-state ozone concentration; [NO₃]_{ss} is the simulated steady-state NO₃ radical concentration; and τ is the chamber mean residence time and can be calculated as the total chamber volume divided by the incoming/outgoing flow rate. The steady-state OH radical concentration ([OH]_{ss}) is derived by solving Equation 1. The yield of MACR from the ozonolysis pathway ($Y_{MACR \leftarrow O_3}$) is taken as 40.8%.²⁷ The yield of MACR from the NO₃ oxidation ($Y_{MACR \leftarrow NO_3}$) is taken as 12.6% although it may vary with the bimolecular lifetime of nitrooxy alkylperoxy radicals.²⁸ Note that uncertainties associated with the prescribed MACR yields from the ozonolysis and NO₃-oxidation of isoprene are small, as these two pathways account for less than ~12% of the overall isoprene reactivity. The molar yield of MACR from the OH oxidation of isoprene is thus given by

$$\begin{aligned} Y_{\text{MACR}\leftarrow\text{OH}} &= \left(k_{\text{MACR}+\text{OH}}[OH]_{\text{ss}}[\text{MACR}]_{\text{ss}} + k_{\text{MACR}+\text{O}_3}[O_3]_{\text{ss}}[\text{MACR}]_{\text{ss}} + k_{\text{MACR}+\text{NO}_3}[\text{NO}_3]_{\text{ss}}[\text{MACR}]_{\text{ss}} \\ &+ \left[\text{MACR}\right]_{\text{ss}} \big/ \tau - Y_{\text{MACR}\leftarrow\text{O}_3} k_{\text{ISOP}+\text{O}_3}[O_3]_{\text{ss}}[\text{ISOP}]_{\text{ss}} \end{aligned}$$

Uncertainties in the calculated yields mainly arise from the systematic errors in the measurements, the calculation of steady-state OH concentrations, and the estimation of the fraction of ISOPOO radicals reacting with NO. These individual uncertainties were further propagated using the variance formula to yield the overall uncertainties, as described in supplemental information section "uncertainties in the yields calculation." The expression of the MVK yield can be derived analogously,

 $-Y_{MACR \leftarrow NO_3} k_{ISOP + NO_3} [NO_3]_{ss} [ISOP]_{ss}) / (k_{ISOP + OH} [OH]_{ss} [ISOP]_{ss})$ (Equation 3)

see details given in supplemental information section "calculation of MVK yields from the OH oxidation of isoprene in the continuous-flow mode."

Figure 2 shows the measured yields of MACR and MVK scaled by the fraction of their precursors, i.e., β-ISOPOO radicals, that react with NO as a function of the ISOPOO bimolecular lifetime. We apply the scaling factor $f_{\beta\text{-ISOPOO}+NO}$ here in order to visualize the β -ISOPOO radical dynamics as a synergic result of the interconversion and isomerization of all ISOPOO radicals. The underlying assumption about the $f_{\text{B-ISOPOO+NO}}$ factor is that MACR and MVK are exclusively produced from reactions of corresponding β-ISOPOO precursors with NO. We caution that this assumption may introduce a slight overestimation of the scaled yields (by less than \sim 5%) under NO-free conditions as MACR and MVK have been suggested as minor products from β -ISOPOO+HO $_2$ reactions. ²⁹ The ISOPOO bimolecular lifetime ($au_{bimolecular}$) is primarily controlled by reactions of ISOPOO radicals with NO and HO2. Under moderate-to-high-NO conditions investigated here (~1-50 ppb), the dominate fate of ISOPOO radicals is to react with NO, and $\tau_{bimolecular}$ is calculated from the measured steady-state NO concentrations. For experiments with sub-ppb level of NO, HO₂ competes for the ISOPOO reactivity, and uncertainties in the HO₂ simulations likely introduce errors to the resulting $\tau_{\text{bimolecular}}$. However, this uncertainty source is reasonably constrained by the agreement (<9.1%) between the model-predicted steady-state OH concentration and that calculated from direct measurements via Equation 1, given that the HO_x cycling in the system is essentially governed by two well-quantified reactants, NO and H₂O₂ (as OH sources), through H₂O₂ + $OH \rightarrow HO_2 + H_2O$ and $HO_2 + NO \rightarrow OH + NO_2$ reactions.³⁰

The yields of MACR (24.6% \pm 1.1%) and MVK (33.0% \pm 2.0%) at short ISOPOO bimolecular lifetimes ($\tau_{\rm bimolecular}$ < 20 ms) lie within the range of previous measurements, i.e., 23.5% \pm 4.5% for MACR and 34.3% \pm 9.7% for MVK. ^{19–24} While these





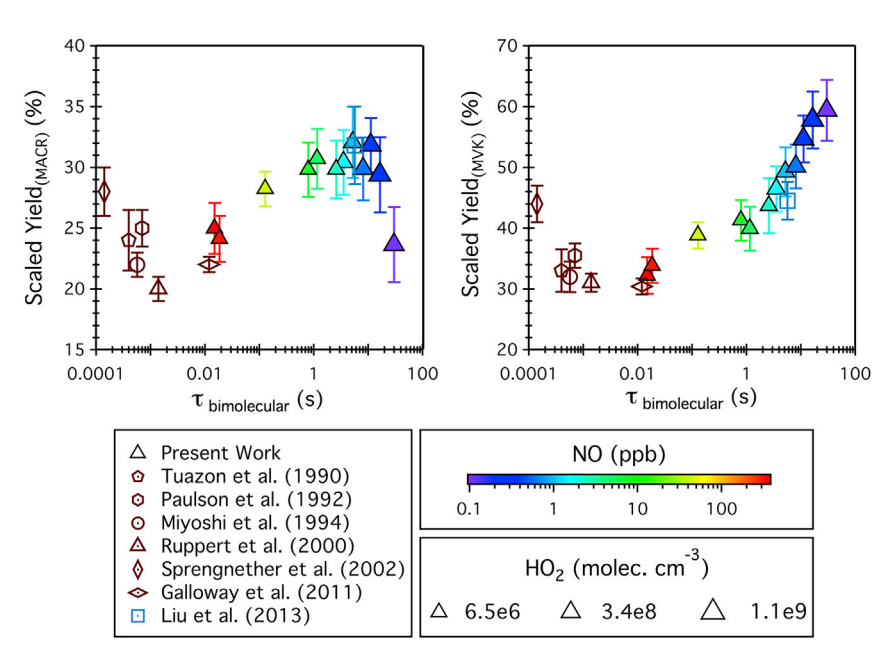


Figure 2. Molar yields of MACR and MVK from the OH-initiated oxidation of isoprene scaled by $f_{\beta\text{-ISOPOO+NO}}$ (the fraction of β -ISOPOO radicals reacting with NO) as a function of the bimolecular lifetime, $\tau_{\text{bimolecular}} = 1/(k_{\text{ISOPOO+NO}}[\text{NO}]_{\text{ss}} + k_{\text{ISOPOO+HO2}}[\text{HO}_2]_{\text{ss}})$, of β -ISOPOO radicals with respect to reactions with NO (0.1–300 ppb, denoted by the triangle color) and HO₂ (10⁶–10⁹ molecules cm⁻³, denoted by the triangle size)

Also plotted are the reported yields with associated uncertainties from a number of previous chamber studies.

earlier measurements ^{19–24} were taken at a lower temperature (295–303 K) compared with the present work (306 K), temperature has a minimal influence on the kinetic distribution of ISOPOO radicals and hence the MACR and MVK yields, when bimolecular reactions with NO dominate the ISOPOO reactivity, see supplemental information section "effect of temperature on the MACR and MVK yields" and Figure \$2 for more details.²⁶ With the branching ratio of 0.88 for the formation of β -ISOPO alkoxy radicals from the β -ISOPOO+NO reaction at 306 K and 0.83 atm, 16 the fractional distributions of β -(4-OH, 3-OO)-ISOPOO (as the MACR precursor) and β -(1-OH,2-OO)-ISOPOO (as the MVK precursor) at nearly the kinetic limit are estimated as \sim 0.26 and \sim 0.37, respectively, accounting for over half of the isoprene carbon. Both MACR and MVK yields increase rapidly as τ_{bimolecular} exceeds 0.1 s, indicating a transition from the kinetic distribution of ISOPOO radicals to their equilibrated distribution, which favors β-ISOPOO isomers as they can be stabilized by the strong internal hydrogen bond. The yield data taken in the presence of ~ 1 ppb NO by Liu et al.²⁹ fall within our measurement range at the intermediate bimolecular lifetime ($\tau_{bimolecular} = \sim 6$ s). The higher temperature (306 K) used in this work could accelerate the O₂ dissociation and hence ISOPOO interconversion, resulting in an enhanced production of MACR and MVK by 3.3% and 0.6%, respectively, compared with the measurements performed at 298 K by Liu et al.²⁹ The MACR yields maximize at $\tau_{\text{bimolecular}}$ = $\sim\!1\text{--}10~\text{s}$ and then decline with further increase in $\tau_{\text{bimolecular}}$. This downward turn is caused by the rapid H-shift isomerization of the Z- δ -(4-OH,1-OO)-ISOPOO radical ($\tau_{isomerization}$ = \sim 0.2 s at 306 K) that outcompetes the bimolecular reactions and effectively depletes the MACR precursor through continuous O2 addition and dissociation reactions. The MVK yields, on the other hand, continuously rise with increasing bimolecular lifetime, reaching $59.4\%~\pm~5.0\%$ at $\tau_{bimolecular}$ of ${\sim}30$ s. Such a near-linear upward trend suggests



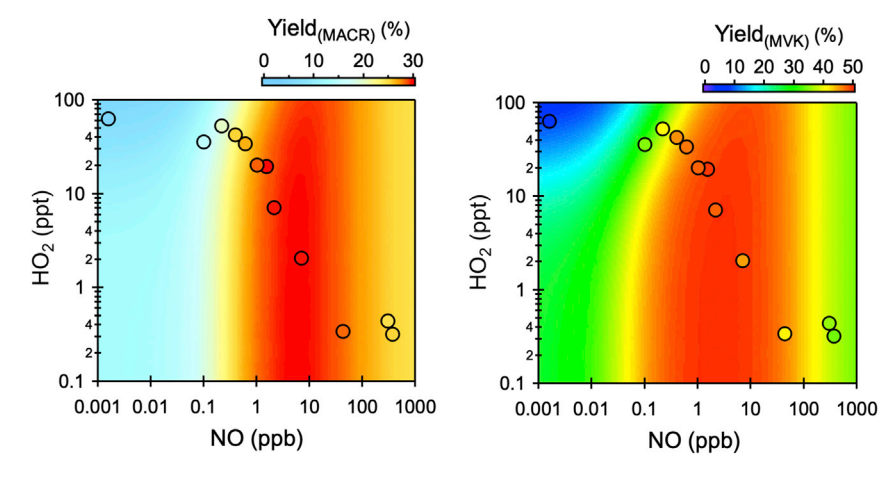


Figure 3. Comparison of the chamber measured molar yields (points) of MACR and MVK from the OH-initiated oxidation of isoprene with model predictions using the updated Caltech Isoprene Mechanism over a range of NO $(0.01-1,000~{\rm ppb})$ and HO₂ $(0.1-100~{\rm ppt})$ concentrations

that the ISOPOO isomerization rate in the 1-OH system is significantly lower than $\sim 10^{-2}~\text{s}^{-1}$, and bimolecular reactions with NO and HO₂ remain the dominant exit channels in the 1-OH system under all experimental conditions investigated here.

Constraining the ISOPOO interconversion kinetics with yield measurements

Measurements of MACR and MVK yields in this study constitute a unique dataset that can be used to constrain the ISOPOO interconversion kinetics that has been recently developed in the Caltech Isoprene Mechanism (CIM, https://data.caltech. edu/records/247). 16 Here the yields of MACR and MVK are used to probe independently the ISOPOO dynamics in the 4-OH and 1-OH systems (see chemical structures given in Figure 1), respectively. Box model simulations with operating mechanisms taken from CIM can reproduce the measured MACR yields within $\pm 12\%$ uncertainties over the entire spectrum of bimolecular reactivities (Figure S3). For the 1-OH-adduct system, the ISOPOO interconversion kinetics were fine-tuned to optimally fit the measurements taken by this work and Teng et al. 17 Specifically, the branching to β-(1-OH,2-OO)-ISOPOO was reduced by 20%, and the branching ratios to E- δ -(1-OH,4-OO)-ISOPOO and Z- δ -(1-OH,4-OO)-ISOPOO became \sim 1.1 and ~5 times of the CIM originals, respectively; see best-fit parameters in Table S1. The O_2 removal rate from Z- δ -(1-OH,4-OO)-ISOPOO was reduced by \sim 40% according to the theoretical calculation by Peeters et al. ²⁶ These mechanistic updates result in a closer agreement (within 14%) between the predicted and measured MVK yields, as shown in Figure \$3. It is important to note that with the updated CIM, the simulated yields of hydroxy nitrates as a function of the ISOPOO bimolecular lifetime generally agree with the measurements by Teng et al., 17 despite an underestimation of the β -1,2-hydroxy nitrate by less than 18% at short ISOPOO bimolecular lifetimes ($\tau_{bimolecular} < \sim 0.1$), as shown in Figure S4.

Simulated yields of MACR and MVK with the updated CIM over a range of NO (0.001-1,000~ppb) and HO_2 (0.1-100~ppt) levels are shown in Figure 3. In contrast to the normalized yields shown in Figure 2, the actual yields reflect the competition between reactions of the ISOPOO radicals with NO and HO_2 as two primary bimolecular partners. This is particularly evident for the chemical regime where HO_2 impacts the ISOPOO bimolecular reactivity, and as a result, the actual yields of MACR and MVK are much lower than the scaled yields in Figure 2. Both MACR and MVK exhibit strong dependence on the NO level, with the maximum yields appearing





in the presence of $\sim\!1-100$ ppb NO. In this NO range, the repetitive O_2 addition and dissociation reactions effectively convert the bulk of the ISOPOO radical pools to the thermally more stable β -ISOPOO isomers. Additionally, the subsequent β -ISOPOO+NO reactions outcompete all other bimolecular and isomerization processes, thereby maximizing the formation potential of MACR and MVK. The HO $_2$ dependence of MVK yields as NO falls below 0.1 ppb is simply a result of competing bimolecular reactions of the β -(1-OH,2-OO)-ISOPOO precursor with HO $_2$ versus NO. On the contrary, negligible dependence of MACR yields on HO $_2$ is observed at low NO levels. This is primarily due to the rapid isomerization of the Z- δ -(4-OH,1-OO)-ISOPOO radical ($\tau_{isomerization} = \sim$ 0.2 s at 306 K), which constitutes the predominant outflow of all 4-OH-ISOPOO fluxes at longer peroxy bimolecular lifetimes. For simulations with the maximum level of HO $_2$, i.e., 100 ppt, the isomerization process is already nearly two orders of magnitude faster than the reactions with HO $_2$, and as a result, further decreases in HO $_2$ concentrations will have a negligible impact on the simulated MACR yields.

Comparison of simulated vertical profiles with aircraft measurements

The updated CIM was incorporated into an observationally constrained box model and validated against airborne measurements of MACR and MVK taken by the Trace Organic Gas Analyzer (TOGA) 31 during the Southeast Atmospheric Studies (SAS) and the Atmospheric Tomography Mission (ATom). These two major campaign efforts surveyed the atmospheric composition from the remote environment to regions at the intersection of human activities and natural processes. 32,33 Taken together, SAS and ATom covered a broad range of NO (5 ppt–1.9 ppb) and HO $_2$ (3.3–74 ppt) levels, corresponding to a peroxy bimolecular lifetime of $\sim\!2$ –300 s. In addition, a wide span of meteorological conditions was sampled during the two campaigns (T \sim 276–299 K and P \sim 0.6–1 \times 10 5 Pa), allowing for testing whether the updated CIM is applicable to the actual atmosphere across different climate zones.

The SAS dataset was selected from three research flights that sampled an array of trace species and radicals over the Eastern US during June 2013. Figure 4 shows the flight tracks, and the TOGA measured vertical profiles of MACR and MVK, with measurement uncertainties of 20% and 30%, respectively. A gradual decline in the concentrations of MACR and MVK with increasing altitude is observed, as a reflection of the short atmospheric lifetimes of both compounds and their precursor isoprene (\sim 4.9, \sim 6.4, and \sim 1.4 h, respectively, at 298 K). Compared with the basecase simulation where MACR and MVK are produced from the isoprene OH oxidation with fixed yields of 22.6% and 33.6%, respectively, the inclusion of the peroxy interconversion mechanism significantly enhances the predicted levels of MACR and MVK by 23%-54% and 57%-79%, respectively (Figure S5). The extent of enhancement depends mainly on the levels of NO and HO₂, which together control the bimolecular lifetime of RO2 radicals and therefore the competitiveness of the RO_2 interconversion in regulating the abundance of β -ISOPOO radicals, as well as the fraction of the RO₂+HO₂ reaction that leads to a small amount of MACR and MVK under low NO conditions. Near the surface ($\sim 0.3-0.5$ km above ground level), simulations with the updated CIM agree closely with observations but overestimate MACR levels by \sim 20%. Constraining HO₂ as the model input to corresponding measurements taken by the chemical ionization mass spectrometer³⁴ enables much improved predictions of MACR across all altitudes (Figures 4A and S5A). In the free troposphere (\sim 1.0–1.5 km), the box model with updated CIM reproduces the vertical profiles of MACR, while it underestimates the MVK concentrations by ~35%, which is near the TOGA measurement uncertainty. This is likely because



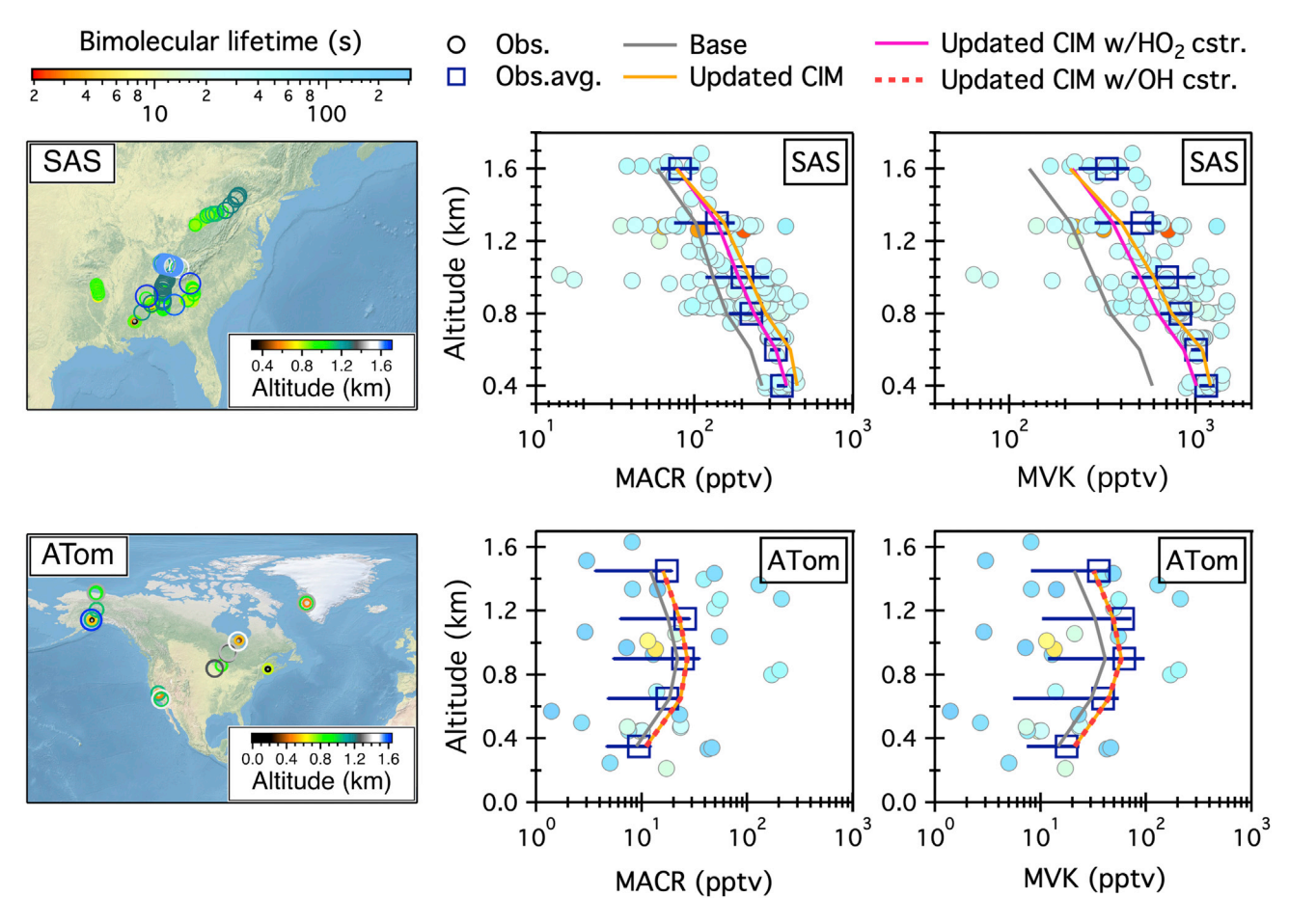


Figure 4. Vertical profiles of MACR and MVK over North America and Greenland collected from SAS (top) and ATom (bottom) campaigns

Each datapoint (denoted by the circle marker) has a color-coded bimolecular lifetime with respect to reactions with NO and HO₂. The observationally constrained box model sampled the air in the same manner as the aircraft measurements. The point-to-point comparison between simulations and measurements is given in Figure S6. Data are grouped in 0.2 or 0.3 km bins. The measurement average within each bin is represented by the square marker, with the horizontal line as the interquartile range of the measurement. Mean values of simulations are represented by colored lines (solid gray: simulations with the base mechanism that prescribes fixed yields, i.e., 22.6% MACR and 33.6% MVK, from isoprene OH oxidation in the presence of NO_x; solid orange: simulations with the updated CIM; solid magenta: SAS simulations with the updated CIM and HO₂ constrained to measurements; and dashed red: ATom simulations with the updated CIM and OH constrained to measurements).

the MACR production is insensitive to HO_2 levels, as the δ -ISOPOO radical isomerization channel contributes to the majority of the carbon outflow in the 4-OH system at extended peroxy bimolecular lifetimes.

The ATom dataset was selected from ATom #1, #3, and #4 flights taken over the Northern Hemisphere from spring to fall during 2016–2018. As shown in Figure 4, these flights sampled the air over Greenland, Alaska, as well as the inner land and coastal areas of North America. Compared with the SAS measurements that focused on the Southeast US, the ATom dataset covers a much larger span of geographic and climate conditions. Due to these surface heterogeneities and meteorological variations that affect the isoprene emissions and chemistry, the compiled vertical profiles of MACR and MVK scattered widely over the sub-ppb range (\sim 1–300 ppt). Despite the missing altitude trends, these measurements complement the SAS dataset by extending the average peroxy bimolecular lifetime from \sim 25 to \sim 101 s. The simulated average concentrations of MACR and MVK match corresponding observations within 14.6% and 15.7%, respectively, across all altitudes in the boundary layer





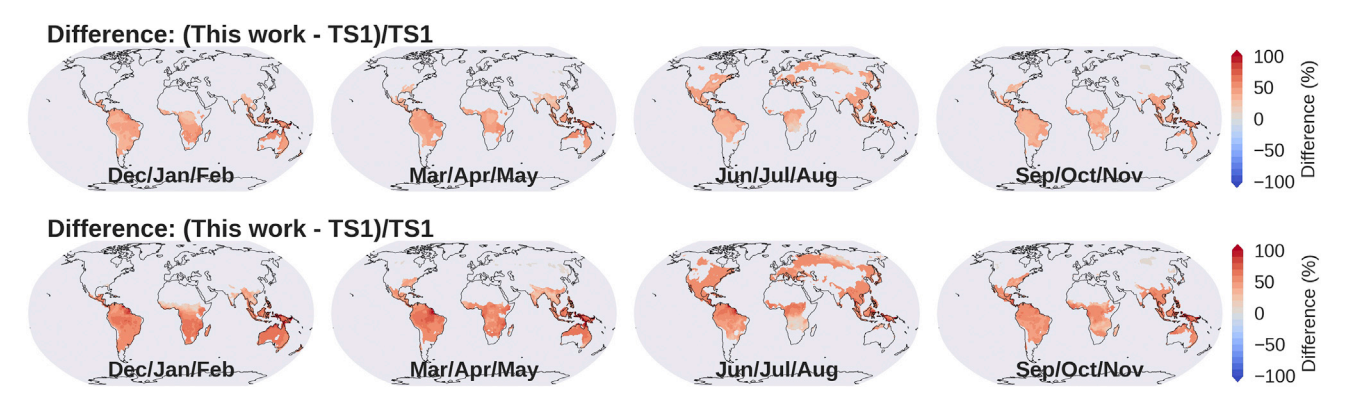


Figure 5. CAM-chem sensitivity analysis of the influence of the isoprene ISOPOO interconversion chemistry on the seasonal-average surface concentrations of MACR (top row) and MVK (bottom row) over the vegetated continents in 2016

Comparison was performed between the updated Caltech Isoprene Mechanism by this work and the original MOZART-TS1 mechanism in CAM-chem.

(Figures 4B and S5B). It is interesting to note that model simulations of MVK at higher altitudes are also biased low although to a much lesser extent compared with the SAS simulations. The underprediction of MVK aloft, or the total of MACR and MVK in general, is likely caused by the excessive atmospheric aging and transport that deviate their mass balance from the initial steady state. In addition to MACR and MVK, the model-predicted HO₂ levels agree reasonably with measurements taken via laser-induced fluorescence, 35 with the best-fit slope of 0.93 on the observation versus simulation scatterplots, as shown in Figure S7. Simulated OH levels are lower by 46.7% on average compared with the measurements, consistent with Brune et al. 35 showing that OH observations exceeded modeled values by \sim 40%. Nevertheless, our model sensitivity analysis suggests that such OH variations have a limited effect on the simulated vertical profiles of MACR and MVK (Figure 4B). Overall, the level of agreement between the observed and modeled vertical profiles demonstrates that the updated isoprene peroxy kinetics operate effectively within the temperature range investigated over continental air masses with little to moderate human influence.

Atmospheric implications

We performed a sensitivity analysis using the Community Atmosphere Model with Chemistry (CAM-chem) version 2.1.0 to assess how the ISOPOO dynamics affect the temporal and spatial distributions of MACR and MVK worldwide. Figure 5 compares the predicted seasonal-average surface concentrations of MACR and MVK in 2016 using the default MOZART-TS1 mechanism versus the updated CIM. The MOZART-TS1 mechanism prescribes a fixed yield of 21.6% for MACR and 33.6% for MVK, respectively, from the OH-initiated oxidation of isoprene, whereas in the updated CIM, the production of MACR and MVK is a synergistic result of competing unimolecular and bimolecular reactions that govern the population distribution of the six ISOPOO radicals. Upon incorporating the ISOPOO interconversion chemistry into CAM-chem, the vast majority of vegetated continents across the world show a remarkable increase in the surface levels of MACR and MVK. The largest increase appears in tropical rainforests (e.g., Pacific Islands and Amazonia), where the surface concentrations of these two species nearly double due to rich isoprene emissions and low-to-moderate NO_x levels. Even in developing regions with frequent occurrence of pollution episodes featuring hundreds of ppb NO_x (e.g., East and Southern Asia), \sim 30%–70% increases in MACR and MVK concentrations are still predicted during the summer season. This suggests that in most vegetated areas of the world, the isoprene peroxy interconversion chemistry operates efficiently and competitively,





and as such, the ISOPOO distribution is closer to their thermal equilibrium that favors the production of MACR and MVK than the kinetic distribution created in classical high- NO_x chamber experiments.

The enhanced production of MACR and MVK at intermediate NO levels (~500 ppt $-\sim$ 10 ppb) suppresses the HO_x radical regeneration and recycling from isoprene photooxidation. When the bulk of ISOPOO radical pools is channeled through the formation of MACR and MVK, the reaction fluxes distributed to the branch of δ -ISO-POO radicals are consequently reduced. Compared with the default MOZART-TS1 mechanism that prescribes a fixed 40% yield to the lumped δ -ISOPOO radical, the actual fraction of δ -ISOPOO radicals can be as low as \sim 5% at their thermal equilibrium distribution. Emerging evidence suggests that isomerization of δ -ISOPOO radicals followed by a cascade of reactions, predominantly the photolysis of hydroperoxyl aldehydes, constitutes a direct source of HO_x radicals.^{36,37} While reaction pathways leading to MACR and MVK also contribute to HO₂ radicals, this HO₂ production mechanism is not unique to the β -ISOPOO channel. In fact, an equal amount of HO_2 radicals can be likewise produced through the δ -ISOPOO+NO reactions. Further oxidation of MACR and MVK can be considered as OH neutral or even positive overall, depending on the HO₂-to-OH conversion efficiency, but the limited amount of OH preserved or regenerated falls far short from compensating the fraction being lost due to the suppression of the δ -ISOPOO isomerization pathway. The daytime average HO_x mixing ratios over the vegetated continents can decrease by up to \sim 5% when the δ -ISOPOO channel is less favored at extended bimolecular lifetimes, as shown in Figure S8. The suppressed regeneration and recycling of HO_x radicals further result in a reduction in the surface O_3 accumulation, in the tropical region in particular, as shown in Figure S9.

The NO-dependent MACR yields characterized in this work will aid in a more accurate estimation of the isoprene-derived SOA budget from local to global scales. At present, most chemical transport models simulate the SOA formation from isoprene photooxidation by parameterizing the chamber-derived isoprene SOA yields with the "two-product" or "volatility basis set" approach, e.g., a fixed ~3% isoprene SOA yield in the presence of NO_x and 10 μg m⁻³ absorbing organic aerosols.³⁸ Recent chamber experiments have suggested that SOA generated from isoprene photooxidation with NO_x is essentially derived from the MACR photochemistry.³⁹ The mass yield of SOA from the OH oxidation of MACR ranges from $\sim 5\%$ to \sim 39%, depending on the NO $_2$ to NO ratio (in the range of 1.7–10). 40 To capture the heterogeneity in the spatial distribution of isoprene SOA, 3D models are suggested to first parameterize the MACR yields from isoprene photooxidation as a function of NO and then the SOA yields from the MACR+OH reaction as a function of the NO/NO₂ ratio. Taking the southeastern US as an example, the MACR yield increases by ~44% on average when the ISOPOO interconversion chemistry is accounted for. Such an increase will result in a ~2%-17% SOA enhancement in the presence of moderate-to-high level NO $_{\rm x}$ (e.g., NO \sim 0.5–50 ppb and $NO_2 > 10 \text{ ppb}$).

As the major first-generation products that account for up to $\sim 80\%$ of the oxidized carbon formed from isoprene photochemistry, MACR and MVK serve as tracers in probing the fate of isoprene under vastly different conditions spanning from remote to urban environments. The measured MACR and MVK yields as a function of varying peroxy bimolecular lifetimes in this work provide strong constraints on the kinetics of the ISOPOO interconversion and their subsequent isomerization processes. While further investigations toward a carbon mass closure are





warranted, the present study clearly demonstrates the widespread operation of the ISOPOO dynamics in the present atmosphere. The implication is that an incremental change in the NO_x concentration above the background level will result in an appreciable perturbation in the isoprene oxidation product distribution with associated impacts on the radical cycling and the production of ozone and organic aerosols. Looking to the future, projected reductions in global anthropogenic emissions will further enhance the importance of isoprene chemistry in modulating the chemical composition and oxidative capacity of the atmosphere.

EXPERIMENTAL PROCEDURES

Resource availability

Lead contact

Further information and requests for resources should be directed to and will be fulfilled by the lead contact, Xuan Zhang (xzhang87@ucmerced.edu).

Materials availability

This study did not generate new materials.

Data and code availability

All data and codes are available from the lead contact upon request.

Chamber experiments and analytical measurements

Experiments were conducted in the 10 m³ NCAR Atmospheric Simulation Chamber.³⁰ Prior to each experiment, the chamber was flushed with purified dry air from an ultra-high purity zero air generator (Model 737, Aadco Instruments) for >12 h until ozone, and NO_x levels were below 1 ppb. During the operation of the steady-state continuous-flow mode, the chamber was constantly flushed with purified dry air at 40 L min⁻¹, which resulted in an average chamber residence time of 4.17 h. The incoming and outgoing flows were balanced by a feedback control system that maintains a constant internal pressure that is 1.2–4.9 \times 10⁻⁴ atm above ambient. Hydrogen peroxide was used as the OH source ($H_2O_2 + hv \rightarrow 2OH_1$, $J_{H_2O_2} \sim 3.93 \times 10^{-7} \text{ s}^{-1}$). Specifically, a 20 mL syringe (Norm-Ject, Henke-Sass Wolf) held on a syringe pump (Model 100, KDScientific) kept at \sim 4°C was used to deliver the H₂O₂ solution (1 wt %, Sigma Aldrich) into a glass bulb that was gently warmed at \sim 32°C. The liquid delivery rate was sufficiently slow (200 μ L min⁻¹) that all the H₂O₂ vapor was released into the glass bulb through evaporation of a small droplet hanging on the needle tip. An air stream (5 L/min) swept the H₂O₂ vapor into the chamber, resulting in an inflow mixing ratio of ~1.3 ppm. Constant NO injection flow in the range of \sim 1–100 ppb was achieved by diluting the gas flow from a concentrated NO cylinder (NO = 133.16 ppm, balance N_2). Similarly, isoprene from a concentrated cylinder ($C_5H_8 = 531$ ppm, balance N_2) was constantly diluted by the flushing air to achieve an inflow mixing ratio of ~20 ppb. As reactant-laden air was continuously flowing through the chamber, it took approximately three turnover times (~12.5 h) for all reactants to reach steady state in the chamber. Figure S1 shows the temporal profiles of NO_x , O_3 , and isoprene for ten experiments operated in the continuous-flow mode. Once the concentration of all reactants was stable in the dark, photooxidation was initiated by irradiating the chamber with 128 fluorescent lights ($J_{NO_2} \sim 1.27 \times 10^{-3} \text{ s}^{-1}$). It generally took $\sim 16 \text{ h}$ for the chamber air contents to establish the final steady state, where mass balance was achieved for all species through inflow supply, outflow dilution, and chemical production and removal. Two static experiments were performed for the measurements of MACR and MVK yields under high-NO conditions. H₂O₂ was used as the OH source by





evaporating 133 μ L of 30 wt % aqueous solution into the chamber with 5 L/min of purified air for \sim 120 min, resulting in an approximate starting concentration of 4 ppm. ^{41–43} Isoprene and NO were injected into the chamber using the cylinder sources described above to achieve initial concentrations of \sim 20 ppb and >300 ppb, respectively. One static experiment in the absence of NO was also conducted to examine the formation of MACR and MVK under NO_x-free conditions. Injections of H₂O₂ and isoprene followed the same protocols as described in high-NO experiments. The chamber air contents were allowed to mix for \sim 60 min before the onset of irradiation.

A suite of instruments was used to monitor gas-phase constituents in the chamber outflow. O₃ was monitored by absorption spectroscopy (Model 49, Thermo Scientific). NO_x was monitored by chemiluminescence (Model CLD 88Y, Eco Physics). In addition, a customized high sensitivity chemiluminescence instrument with a detection limit of ~25 ppt was used to detect NO at sub-ppb level. Mixing ratios of isoprene, MACR, and MVK were measured using a gas chromatograph with a customized Peltier-cooled pre-concentrator and a flame ionization detector (GC-FID, Model G1530A, Agilent). Artifacts in the measured MACR and MVK signals can be produced through thermal decomposition of isoprene oxidation products, such as the peroxides and epoxides, on contact with hot metal surface.⁴² A cold trap was thus used to eliminate these interferences in the interpretation of the GC-FID data. Specifically, a 1-m section of coiled Teflon tubing was submerged in a low temperature ethanol bath ($-40^{\circ}\text{C} \pm 2^{\circ}\text{C}$) to trap oxidized products less volatile than MACR and MVK after steady state was established in the chamber. The quantification of MACR and MVK was then based on the GC-FID measurements downstream of the cold trap.

Aircraft observations during SAS and ATom

Airborne measurements of MACR and MVK were taken by the TOGA instrument (supplemental information section "MACR and MVK measurements by TOGA during SAS and ATom")31 during the SAS and ATom campaigns. The Nitrogen, Oxidants, Mercury, and Aerosol Distributions, Sources and Sinks (NOMADSS) experiment under the umbrella of the SAS campaign took place in the summer of 2013. The experiment flew 19 research flights with the NSF/NCAR C-130 aircraft over the southeastern US based out of Smyrna, TN. Measurements discussed in this study were extracted from flights taken on 20, 22, and 29 June over parts of rural Eastern US covered with various vegetation types. For these three flights, complete datasets of meteorological parameters, water vapor, CO, SO₂, NO_x, HO₂, O₃, HONO, methane, VOCs, and photolysis frequencies were downloaded from the SAS data archive (https://data.eol.ucar.edu/master_lists/generated/sas/). The ATom campaign was designed to map the remote atmosphere composition over the globe. It consisted of four individual field campaigns conducted in each of four seasons, over a 2-year period, using the NASA DC-8 research aircraft to sample the atmosphere from \sim 180 m to \sim 12 km above sea level from the Arctic to the Antarctic over the Pacific and Atlantic Oceans. Measurements discussed in this study were selected from flights over North America and Greenland (data are accessible at https://doi.org/10.3334/ORNLDAAC/1581), where the influence of ocean emissions on the measured vertical profiles of trace species is minor.

0D box model

Chamber experiments were simulated by a box model with the MCMv3.3.1 (accessible at http://mcm.york.ac.uk). Initial model inputs include temperature (306 K), local pressure (8.6 \times 10⁴ Pa), relative humidity (5%), light intensity





 $(J_{NO_2}=1.27\times10^{-3}~{\rm s}^{-1})$, chamber mean residence time (4.17 h), and continuous inflow of ${\rm H_2O_2}$ (\sim 0.6–0.8 ppm), NO (\sim 0.7–96 ppb), and isoprene (\sim 19–21 ppb). The predicted steady-state HO₂ concentrations are used for the calculation of the lifetime of ISOPOO radicals with respect to reactions with HO₂ and NO, as well as the scaling factor $f_{\rm B-ISOPOO+NO}$ applied to the measured yields shown in Figure 2. The updated CIM was incorporated into the box model framework for the prediction of MACR and MVK yields from the isoprene OH oxidation under a range of NO and HO₂ levels shown in Figure 3. The model was operated with constant radical levels, including OH (2 × 10^6 molecules cm⁻³), HO₂ (0.1–100 ppt), NO (0.01–1,000 ppb), NO₂ (2 ppb), and NO₃ (0 ppb), in order to limit the impact of the HO_x/NO_x cycling inherent in the isoprene chemistry on the predicted product yields.

In addition to simulating chamber experiments, the box model was also employed to simulate the horizontal and vertical distributions of MACR and MVK observed during the SAS and ATom campaigns. The model was constrained by a comprehensive suite of *in situ* measurements that characterize the meteorological conditions and the chemical composition of air masses sampled by the aircraft, including temperature, humidity, pressure, CO, NO $_{x}$, O $_{3}$, SO $_{2}$, HONO, biogenic and anthropogenic VOCs (including isoprene), and photolysis frequencies of O $_{3}$, NO $_{2}$, NO $_{3}$, HONO, HCHO, and H $_{2}$ O $_{2}$ (see details given in Table S2). Predicted diurnal steady-state levels of MACR and MVK are compared with the TOGA measurements taken during ATom and SAS flights. Also included in the comparison are simulated and measured HO $_{2}$ concentrations cross all altitudes, as shown in Figure S7.

CAM-chem

Sensitivity simulations were performed using the CAM-chem model, a component of the Community Earth System Model (CESM2.1.0), with the MOZART-TS1 chemical mechanism, 45 which contains 221 species and 528 reactions. The specified dynamics component set (FCSD) was used as the default model settings except for the following: 32 vertical levels were used instead of 56; the meteorology was nudged to Modern-Era Retrospective analysis for Research and Applications; Version 2 (MERRA2) interpolated to 32 levels; and the biogenic emissions were expanded to include more species from the Model of Emissions of Gases and Aerosols from Nature (MEGAN) inventory. Further details of these changes are provided in Schwantes et al. 46 In the MOZART-TS1 chemical mechanism, OH oxidation of isoprene yields two peroxy radicals, one of which further reacts with NO leading to 22.6% MACR and 33.6% MVK. Updates to the base mechanism for this study include the following: isoprene reacts with OH to form 4 OH-adducts, which react with O_2 to form 6 hydroxy peroxy radicals; the O_2 addition/removal rates are from the Leuven Isoprene Mechanism²⁶ for the 1-OH-adduct system and the CIM for the 4-OHadduct system; and each of the hydroxy peroxy radicals react with NO, HO₂, NO₃, CH₃O₂, and CH₃CO₃, and isomerize. The isomer-dependent product yields of MVK and MACR are updated for these peroxy radical bimolecular and isomerization reactions, but all other products remain the same as the MOZART-TS1 chemical mechanism (see the list of reactions given in Table S3). The updated model simulation was spun-up for 7 months from the base simulation, which was spun-up for 2 years

SUPPLEMENTAL INFORMATION

Supplemental information can be found online at https://doi.org/10.1016/j.chempr. 2022.08.003.





ACKNOWLEDGMENTS

The work was supported by the US National Science Foundation grant AGS-2131199. The National Center for Atmospheric Research is operated by the University Corporation for Atmospheric Research under the sponsorship of the US National Science Foundation. Siyuan Wang and Rebecca H. Schwantes were supported in part by the NOAA Cooperative Agreement with the Cooperative Institute for Research in Environmental Sciences, NA17OAR4320101. Kirk Ullmann (Atmospheric Chemistry Observations & Modeling Laboratory, National Center for Atmospheric Research) is acknowledged for the photolysis frequency measurements via the Actinic Flux Spectroradiometer. Ilann Bourgeois, Jeff Peischl, Thomas B. Ryerson, and Chelsea Thompson (Earth System Research Laboratory, National Oceanic and Atmospheric Administration) are acknowledged for the measurements of NO_v and O₃. Glenn S. Diskin (Langley Research Center, National Aeronautics and Space Administration) is acknowledged for the water vapor measurements by the Diode Laser Hygrometer. Thomas F. Hanisco and Jason M. St. Clair (Goddard Space Flight Center, National Aeronautics and Space Administration) are acknowledged for the in situ Airborne Formaldehyde measurements. Kathryn McKain (Earth System Research Laboratory, National Oceanic and Atmospheric Administration) is acknowledged for the methane and carbon monoxide measurements by the Wavelength-Scanned Cavity Ring Down Spectroscopy.

AUTHOR CONTRIBUTIONS

X.Z., P.O.W., G.S.T., and J.J.O. designed the study; X.Z. and J.O. performed the chamber experiments; E.C.A., R.S.H., A.J.H., W.H.B., R.L.M., C.A.C., D.R.B., T.C., B.D., S.R.H., and S.C.W. performed aircraft measurements; X.Z., Z.M., K.E.D., A.P.T., G.S.T., and J.J.O. analyzed the data; S.W., R.H.S. and L.K.E. performed model simulations; X.Z., S.W., Z.M., K.E.D., and R.H.S. prepared the figures; and X.Z., G.S.T., and J.J.O. wrote the manuscript.

DECLARATION OF INTERESTS

The authors declare no competing interests.

Received: February 18, 2022 Revised: May 2, 2022 Accepted: August 3, 2022 Published: August 29, 2022

REFERENCES

- Goldstein, A.H., and Galbally, I.E. (2007). Known and unexplored organic constituents in the Earth's atmosphere. Environ. Sci. Technol. 41, 1514–1521. https://doi.org/10.1021/ es072476p.
- Guenther, A.B., Jiang, X., Heald, C.L., Sakulyanontvittaya, T., Duhl, T., Emmons, L.K., and Wang, X. (2012). The Model of Emissions of Gases and Aerosols from Nature version 2.1 (MEGAN2.1): an extended and updated framework for modeling biogenic emissions. Geosci. Model Dev. 5, 1471–1492. https://doi.org/10.5194/gmd-5-1471-2012.
- 3. Atkinson, R., Baulch, D.L., Cox, R.A., Crowley, J.N., Hampson, R.F., Hynes, R.G., Jenkin, M.E., Rossi, M.J., Troe, J., and IUPAC Subcommittee. (2006). Evaluated kinetic and

- photochemical data for atmospheric chemistry: volume II-gas phase reactions of organic species. Atmos. Chem. Phys. 6, 3625-4055. https://doi.org/10.5194/acp-6-3625-2006
- Lelieveld, J., Butler, T.M., Crowley, J.N., Dillon, T.J., Fischer, H., Ganzeveld, L., Harder, H., Lawrence, M.G., Martinez, M., and Taraborrelli, D. (2008). Atmospheric oxidation capacity sustained by a tropical forest. Nature 452, 737–740. https://doi.org/10.1038/nature06870.
- Paulot, F., Crounse, J.D., Kjaergaard, H.G., Kürten, A., St. Clair, J.M., Seinfeld, J.H., and Wennberg, P.O. (2009). Unexpected epoxide formation in the gas-phase photooxidation of isoprene. Science 325, 730–733. https://doi.org/10.1126/science. 1172910.
- Fuchs, H., Hofzumahaus, A., Rohrer, F., Bohn, B., Brauers, T., Dorn, H.-O., Häseler, R., Holland, F., Kaminski, M., Li, X., et al. (2013). Experimental evidence for efficient hydroxyl radical regeneration in isoprene oxidation. Nat. Geosci. 6, 1023–1026. https://doi.org/10. 1038/ngeo1964.
- Mao, J., Paulot, F., Jacob, D.J., Cohen, R.C., Crounse, J.D., Wennberg, P.O., Keller, C.A., Hudman, R.C., Barkley, M.P., and Horowitz, L.W. (2013). Ozone and organic nitrates over the eastern United States: sensitivity to isoprene chemistry. J. Geophys. Res. Atmos. 118, 256–268. https://doi.org/10.1002/jgrd. 50817.
- Bates, K.H., and Jacob, D.J. (2019). A new model mechanism for atmospheric oxidation of isoprene: global effects on oxidants,

Chem Article



- nitrogen oxides, organic products, and secondary organic aerosol. Atmos. Chem. Phys. 19, 9613–9640. https://doi.org/10.5194/aep-19-9613-2019.
- Claeys, M., Graham, B., Vas, G., Wang, W., Vermeylen, R., Pashynska, V., Cafmeyer, J., Guyon, P., Andreae, M.O., Artaxo, P., et al. (2004). Formation of secondary organic aerosols through photooxidation of isoprene. Science 303, 1173–1176. https://doi.org/10. 1126/science.1092805.
- Froyd, K.D., Murphy, S.M., Murphy, D.M., de Gouw, J.A., Eddingsaas, N.C., and Wennberg, P.O. (2010). Contribution of isoprene-derived organosulfates to free tropospheric aerosol mass. Proc. Natl. Acad. Sci. USA 107, 21360– 21365. https://doi.org/10.1073/pnas. 1012561107.
- Surratt, J.D., Chan, A.W., Eddingsaas, N.C., Chan, M., Loza, C.L., Kwan, A.J., Hersey, S.P., Flagan, R.C., Wennberg, P.O., and Seinfeld, J.H. (2010). Reactive intermediates revealed in secondary organic aerosol formation from isoprene. Proc. Natl. Acad. Sci. USA 107, 6640– 6645. https://doi.org/10.1073/pnas. 0911114107.
- Hewitt, C.N., Ashworth, K., Boynard, A., Guenther, A., Langford, B., MacKenzie, A.R., Misztal, P.K., Nemitz, E., Owen, S.M., Possell, M., et al. (2011). Ground-level ozone influenced by circadian control of isoprene emissions. Nat. Geosci. 4, 671–674. https://doi.org/10.1038/ ngeo1271.
- Lin, Y.-H., Zhang, H., Pye, H.O., Zhang, Z., Marth, W.J., Park, S., Arashiro, M., Cui, T., Budisulistiorini, S.H., Sexton, K.G., et al. (2013). Epoxide as a precursor to secondary organic aerosol formation from isoprene photooxidation in the presence of nitrogen oxides. Proc. Natl. Acad. Sci. USA 110, 6718– 6723. https://doi.org/10.1073/pnas. 1221150110.
- Xu, L., Guo, H., Boyd, C.M., Klein, M., Bougiatioti, A., Cerully, K.M., Hite, J.R., Isaacman-VanWertz, G., Kreisberg, N.M., Knote, C., et al. (2015). Effects of anthropogenic emissions on aerosol formation from isoprene and monoterpenes in the southeastern United States. Proc. Natl. Acad. Sci. USA 112, 37–42. https://doi.org/10.1073/ pnas.1417609112.
- Liu, Y., Brito, J., Dorris, M.R., Rivera-Rios, J.C., Seco, R., Bates, K.H., Artaxo, P., Duvoisin, S., Keutsch, F.N., Kim, S., et al. (2016). Isoprene photochemistry over the Amazon rainforest. Proc. Natl. Acad. Sci. USA 113, 6125–6130. https://doi.org/10.1073/pnas.1524136113.
- Wennberg, P.O., Bates, K.H., Crounse, J.D., Dodson, L.G., McVay, R.C., Mertens, L.A., Nguyen, T.B., Praske, E., Schwantes, R.H., Smarte, M.D., et al. (2018). Gas-phase reactions of isoprene and its major oxidation products. Chem. Rev. 118, 3337–3390. https://doi.org/10. 1021/acs.chemrev.7b00439.
- Teng, A.P., Crounse, J.D., and Wennberg, P.O. (2017). Isoprene peroxy radical dynamics.
 J. Am. Chem. Soc. 139, 5367–5377. https://doi. org/10.1021/jacs.6b12838.
- Orlando, J.J., and Tyndall, G.S. (2012). Laboratory studies of organic peroxy radical chemistry: an overview with emphasis on recent

- issues of atmospheric significance. Chem. Soc. Rev. 41, 6294–6317. https://doi.org/10.1039/C2CS35166H.
- Tuazon, E.C., and Atkinson, R. (1990). A product study of the gas-phase reaction of isoprene with the OH radical in the presence of NOx. Int. J. Chem. Kinet. 22, 1221–1236. https://doi.org/10.1002/kin.550221202.
- Paulson, S.E., and Seinfeld, J.H. (1992). Development and evaluation of a photooxidation mechanism for isoprene.
 J. Geophys. Res. 97, 20703–20715. https://doi. org/10.1029/92JD01914.
- Miyoshi, A., Hatakeyama, S., and Washida, N. (1994). OH radical-initiated photooxidation of isoprene: an estimate of global CO production. J. Geophys. Res. 99, 18779–18787. https://doi. org/10.1029/94JD01334.
- Ruppert, L., and Becker, K.H. (2000). A product study of the OH radical-initiated oxidation of isoprene: formation of C5-unsaturated diols. Atmos. Environ. 4, 1529–1542. https://doi.org/ 10.1016/S1352-2310(99)00408-2.
- Sprengnether, M., Demerjian, K.L., Donahue, N.M., and Anderson, J.G. (2002). Product analysis of the OH oxidation of isoprene and 1, 3-butadiene in the presence of NO.
 J. Geophys. Res. 107, D15. https://doi.org/10. 1029/2001JD000716.
- Galloway, M.M., Huisman, A.J., Yee, L.D., Chan, A.W.H., Loza, C.L., Seinfeld, J.H., and Keutsch, F.N. (2011). Yields of oxidized volatile organic compounds during the OH radical initiated oxidation of isoprene, methyl vinyl ketone, and methacrolein under high-NOx conditions. Atmos. Chem. Phys. 11, 10779– 10790. https://doi.org/10.5194/acp-11-10779-2011
- Peeters, J., Nguyen, T.L., and Vereecken, L. (2009). HOx radical regeneration in the oxidation of isoprene. Phys. Chem. Chem. Phys. 11, 5935–5939. https://doi.org/10.1039/ B908511D.
- Peeters, J., Müller, J.-F., Stavrakou, T., and Nguyen, V.S. (2014). Hydroxyl radical recycling in isoprene oxidation driven by hydrogen bonding and hydrogen tunneling: the upgraded LIM1 mechanism. J. Phys. Chem. A 118, 8625–8643. https://doi.org/10.1021/ jp5033146.
- Nguyen, T.B., Tyndall, G.S., Crounse, J.D., Teng, A.P., Bates, K.H., Schwantes, R.H., Coggon, M.M., Zhang, L., Feiner, P., Milller, D.O., et al. (2016). Atmospheric fates of Criegee intermediates in the ozonolysis of isoprene. Phys. Chem. Chem. Phys. 18, 10241– 10254. https://doi.org/10.1039/C6CP00053C.
- Schwantes, R.H., Teng, A.P., Nguyen, T.B., Coggon, M.M., Crounse, J.D., St. Clair, J.M., Zhang, X., Schilling, K.A., Seinfeld, J.H., and Wennberg, P.O. (2015). Isoprene NO3 oxidation products from the RO2+HO2 pathway. J. Phys. Chem. A 119, 10158-10171. https://doi.org/10.1021/acs.jpca.5b06355.
- Liu, Y.J., Herdlinger-Blatt, I., McKinney, K.A., and Martin, S.T. (2013). Production of methyl vinyl ketone and methacrolein via the hydroperoxyl pathway of isoprene oxidation. Atmos. Chem. Phys. 13, 5715–5730. https://doi. org/10.5194/acp-13-5715-2013.

- Zhang, X., Ortega, J., Huang, Y., Shertz, S., Tyndall, G.S., and Orlando, J.J. (2018). A steady-state continuous flow chamber for the study of daytime and nighttime chemistry under atmospherically relevant NO levels. Atmos. Meas. Tech. 11, 2537–2551. https://doi. org/10.5194/amt-11-2537-2018.
- Apel, E.C., Hornbrook, R.S., Hills, A.J., Blake, N.J., Barth, M.C., Weinheimer, A., Cantrell, C., Rutledge, S.A., Basarab, B., Crawford, J., et al. (2015). Upper tropospheric ozone production from lightning NOx-impacted convection: smoke ingestion case study from the DC3 campaign. J. Geophys. Res. Atmos. 120, 2505–2523. https://doi.org/10.1002/ 2014JD022121.
- Carlton, A.G., de Gouw, J., Jimenez, J.L., Ambrose, J.L., Attwood, A.R., Brown, S., Baker, K.R., Brock, C., Cohen, R.C., Edgerton, S., et al. (2018). Synthesis of the Southeast Atmosphere Studies: investigating fundamental atmospheric chemistry questions. Am. Meteorol. Soc. 99, 547–567. https://doi.org/10. 1175/BAMS-D-16-0048.1.
- Thompson, C.R., Wofsy, S.C., Prather, M.J., Newman, P.A., Hanisco, T.F., Ryerson, T.B., Fahey, D.W., Apel, E.C., Brock, C.A., Brune, W.H., et al. (2021). The NASA atmospheric Tomography (ATom) mission: imaging the chemistry of the global atmosphere. Am. Meteorol. Soc. 103, 1–53. https://doi.org/10. 1175/BAMS-D-20-0315.1.
- 34. Mauldin, R.L., III, Cantrell, C.A., Zondlo, M., Kosciuch, E., Eisele, F.L., Chen, G., Davis, D., Weber, R., Crawford, J., and Blake, D. (2003). Highlights of OH, H2SO4, and methane sulfonic acid measurements made aboard the NASA P-3B during Transport and Chemical Evolution over the Pacific. J. Geophys. Res. 108, 8796. https://doi.org/10.1029/2003JD003410.
- Brune, W.H., Miller, D.O., Thames, A.B., Allen, H.M., Apel, E.C., Blake, D.R., Bui, T.P., Commane, R., Crounse, J.D., Daube, B.C., et al. (2020). Exploring oxidation in the remote free troposphere: insights from atmospheric tomography (ATom). J. Geophys. Res. Atmos. 125, e2019. https://doi.org/10.1029/ 2019JD031685.
- Wolfe, G.M., Crounse, J.D., Parrish, J.D., St Clair, J.M., Beaver, M.R., Paulot, F., Yoon, T.P., Wennberg, P.O., and Keutsch, F.N. (2012). Photolysis, OH reactivity and ozone reactivity of a proxy for isoprene-derived hydroperoxyenals (HPALDs). Phys. Chem. Chem. Phys. 14, 7276–7286. https://doi.org/ 10.1039/C2CP40388A.
- Liu, Z., Nguyen, V.S., Harvey, J., Müller, J.-F., and Peeters, J. (2017). Theoretically derived mechanisms of HPALD photolysis in isoprene oxidation. Phys. Chem. Chem. Phys. 19, 9096–9106. https://doi.org/10.1039/ C7CP00288B.
- Carlton, A.G., Wiedinmyer, C., and Kroll, J.H. (2009). A review of secondary organic aerosol (SOA) formation from isoprene. Atmos. Chem. Phys. 9, 4987–5005. https://doi.org/10.5194/ acp-9-4987-2009.
- Nguyen, T.B., Bates, K.H., Crounse, J.D., Schwantes, R.H., Zhang, X., Kjaergaard, H.G., Surratt, J.D., Lin, P., Laskin, A., Seinfeld, J.H., et al. (2015). Mechanism of the hydroxyl





- radical oxidation of methacryloyl peroxynitrate (MPAN) and its pathway toward secondary organic aerosol formation in the atmosphere. Phys. Chem. Chem. Phys. 17, 17914–17926. https://doi.org/10.1039/
- Chan, A.W.H., Chan, M.N., Surratt, J.D., Chhabra, P.S., Loza, C.L., Crounse, J.D., Yee, L.D., Flagan, R.C., Wennberg, P.O., and Seinfeld, J.H. (2010). Role of aldehyde chemistry and NOx concentrations in secondary organic aerosol formation. Atmos. Chem. Phys. 10, 7169–7188. https://doi.org/10. 5194/acp-10-7169-2010.
- 41. Nguyen, T.B., Crounse, J.D., Schwantes, R.H., Teng, A.P., Bates, K.H., Zhang, X., St. Clair, J.M., Brune, W.H., Tyndall, G.S., Keutsch, F.N., et al. (2014). Overview of the Focused Isoprene eXperiment at the California Institute of Technology (FIXCIT): mechanistic chamber studies on the oxidation of

- biogenic compounds. Atmos. Chem. Phys. 14, 13531–13549. https://doi.org/10.5194/acp-14-13531-2014.
- Schwantes, R.H., McVay, R.C., Zhang, X., Coggon, M.M., Lignell, H., Flagan, R.C., Wennberg, P.O., and Seinfeld, J.H. (2017). Science of the Environmental Chamber. In Advances in Atmospheric Chemistry, J.R. Barker, A.L. Steiner, and T.J. Wallington, eds. (World Scientific), pp. 1–93. https://doi.org/10.1142/ 9789813147355_0001.
- Zhang, X., Schwantes, R.H., Coggon, M.M., Loza, C.L., Schilling, K.A., Flagan, R.C., and Seinfeld, J.H. (2014). Role of ozone in SOA formation from alkane photooxidation. Atmos. Chem. Phys. 14, 1733–1753. https://doi.org/10. 5194/acp-14-1733-2014.
- 44. Wang, H., Gao, Y., Wang, S., Wu, X., Liu, Y., Li, X., Huang, D., Lou, S., Wu, Z., Guo, S., et al.

- (2020). Atmospheric processing of nitrophenols and nitrocresols from biomass burning emissions. J. Geophys. Res. Atmos. 125, e2020. https://doi.org/10.1029/2020JD033401.
- Emmons, L.K., Schwantes, R.H., Orlando, J.J., Tyndall, G., Kinnison, D., Lamarque, J.F., Marsh, D., Mills, M.J., Tilmes, S., Bardeen, C., et al. (2020). The chemistry mechanism in the Community Earth System Model version 2 (CESM2). J. Adv. Model. Earth Syst. 12, e2019. https://doi.org/10.1029/ 2019MS001882.
- Schwantes, R. H., Emmons, L. K., Orlando, J. J., Barth, M. C., Tyndall, G. S., Hall, S. R., Ullmann, K., St. Clair, J. M., Blake, D. R., Wisthaler, A., et al. (2020). Comprehensive isopreneand terpenegas-phase chemistry improvessimulated surface ozone in the southeastern U.S. Atmos. Chem. Phys. 20, 3739– 3776. https://doi.org/10.5194/acp-20-3739-2020.